Rotational Spectroscopy Probes Lone Pair···π-Hole Interactions in Hexafluorobenzene-Tertiary Alkylamines Complexes

Rotational Spectroscopy Probes Lone Pair···π-Hole Interactions in Hexafluorobenzene-Tertiary Alkylamines Complexes

Dingding Lv, Weixing Li,* Luca Evangelisti,* Imanol Usabiaga, Camilla Calabrese, Assimo Maris, Sonia Melandri,* Guanjun Wang, and Mingfei Zhou*

ABSTRACT: We employed microwave spectroscopy to investigate the 1:1 complexes of hexafluorobenzene with trimethylamine and quinuclidine, respectively. These complexes exhibit a C_{3v} symmetry and are stabilized by nitrogen lone pair···π-hole interactions along the C_3 axes. The N···π-center distances were determined to be 3.110(1) and 3.040(2) Å, respectively, which are shorter than that of hexafluorobenzene-ammonia at 3.2685(3) Å. Additionally, the strength of the intermolecular interaction increases with cluster size. While it was initially expected that the electron-donating effect of alkyl groups was responsible for changing the N···π interaction, the symmetry-adapted perturbation theory analysis revealed that, from hexafluorobenzene-ammonia to both hexafluorobenzene-alkylamines, electrostatic interaction actually decreases while dispersion interaction increases and becomes dominant. Interestingly, dispersion interaction decreases while electrostatic interaction increases from C_6F_6–$N(CH_3)_3$ to C_6F_6–NC_7H_{13}. The splitting pattern of the spectra indicates hexafluorobenzene rotates freely relative to its partners along the axis of the N···π-hole interactions.

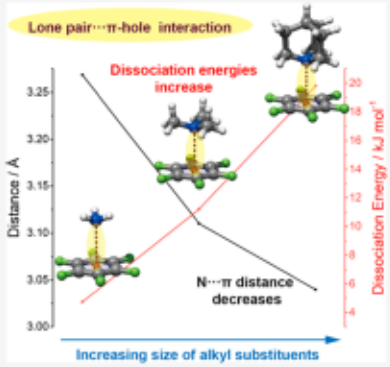

Noncovalent interactions (NCIs) are ubiquitous in nature, governing the molecular structures and thus biochemical functionalities and reactivities, such as maintaining the three-dimensional structures of biomolecules and leading molecular recognitions by the delicate balance between different NCIs on top of the covalently bound structural backbone.[1−3] Great effort has been devoted to the characterization of NCIs and the understanding of their nature.[4−11] NCIs are relatively weak compared to covalent bonds, and accurate characterization of the structure and interaction energy of NCIs experimentally is often facing significant challenges.[12−14] Molecular rotational spectroscopy offers a way to study NCIs on model systems under well-defined jet expansion conditions.[6,7,15] Rotational spectroscopy is directly related to the principal moments of inertia of the molecule including their centrifugal distortion and, therefore, is suited for analysis of geometric structures of weakly bound molecular complexes.[16−19] Recent rotational spectroscopic investigations have unveiled the nature of tetrel,[20] pnictogen,[6] chalcogen,[15] halogen,[21] CH···π,[22] OH···$\pi_{C=C}$,[23] and π-stacking[24] noncovalent interactions.

The lone pair···π hole interaction (lp-π) referring to the stabilizing interaction between a lone pair of electrons and an electron-poor π system was suggested to be responsible for the stabilization of the left-handed helix in the d(CpG) steps of Z-DNA in 1995.[25] The lp-π interactions in the gas-phase clusters of halogenated ethylene and aromatic rings with water,[26−28] ammonia,[29] or formaldehyde[30] molecules have been studied by rotational spectroscopy. Recently, we investigated the lp-π interaction involving the nitrogen lone pair in the hexafluorobenzene (C_6F_6)-ammonia (NH_3) complex.[31] In this study, we report a rotational spectroscopic study on the complexes of C_6F_6 with trimethylamine ($N(CH_3)_3$) and quinuclidine (NC_7H_{13}) to unravel the alkyl substituent effect on the lp-π interactions. The fact that trimethylamine and quinuclidine are better electron donors than ammonia is widely recognized, based on the ordering of their basicity in aqueous solution, which is NH_3 < $N(CH_3)_3$ < NC_7H_{13}.[32−34] The enhanced electron-donating ability can be attributed to the alkyl groups' electron-donating effect.[35,36] Therefore, it is intuitively expected that the strength of lp-π bonding would increase in the complexes of C_6F_6–$N(CH_3)_3$ and C_6F_6–NC_7H_{13}.

Dispersion interactions were often disregarded due to the widespread belief that they are feeble.[37] However, as larger systems contain more pairwise interactions, dispersion increases rapidly.[37,38] Even in molecular dimers, dispersion interactions have been shown to be significant. For example, dispersion is as significant as electrostatic forces in stabilizing naphthol-aromatic ring complexes,[39] and it even dictates the interactions of diadamantyl ether-aromatics complexes.[40] Thus, it is crucial to comprehensively examine the interplay between

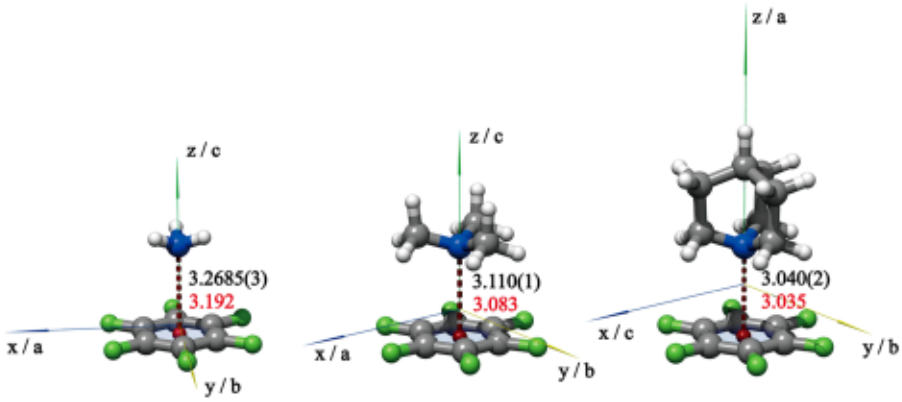

Figure 1. Molecular structures and N··· π-center distances (in Å) for C_6F_6–NH_3, C_6F_6–$N(CH_3)_3$, and C_6F_6–NC_7H_{13}. The distances between the nitrogen atom and the center of the aromatic ring are denoted by the red values for structures calculated at the B3LYP-D4/def2-TZVP level[44] and by black values for experimental results (r_0).

different noncovalent interactions through detailed computational and experimental studies for an understanding of their role in governing the structural arrangement of biological molecules and supramolecular complexes.[41−43]

The theoretically predicted global minimum structures of the complexes of C_6F_6 with $N(CH_3)_3$ and NC_7H_{13}, together with C_6F_6–NH_3, are shown in Figure 1. The ammonia derivatives lie above the aromatic plane of C_6F_6, pointing their nitrogen lone pair toward the center of the ring. Their C_3 symmetry axes coincide with the C_6 axis of C_6F_6, resulting in a molecular C_{3v} symmetry. Consistent with the spectral characteristics of C_6F_6–NH_3,[31] C_6F_6–$N(CH_3)_3$ is also an almost spheric oblate symmetric rotor, characterized by electric dipole moment μ = 1.06 D, while C_6F_6–NC_7H_{13} is a prolate symmetric rotor with μ = 1.79 D. The calculated structural parameters can be found in the Supporting Information (Tables S1−S3).

The rotational spectra of C_6F_6–NC_7H_{13} and C_6F_6–$N(CH_3)_3$ in the 6−18 GHz frequency range are measured using the coaxially oriented beam resonator arrangement (COBRA) Fourier Transform Microwave (FTMW) spectrometer at the University of Bologna.[45−47] A hyperfine structure is observed for both species, as exemplified by the transitions shown in Figure 2a,b, respectively. The spectrum of C_6F_6–NC_7H_{13} is further measured in the low-frequency range by the newly built chirped pulse FTMW Spectrometer (CP-FTMW) at Fudan University, which covers the range from 2 to 8 GHz in a single signal collection event.[11,48,49] The broadband spectra of C_6F_6–$N(CH_3)_3$ in the frequency range of 6−12.5 GHz is measured using a CP-FTMW with a new solid-state amplifier. The experimental details can be found in the Supporting Information. After 1.3 million free induction decay (FID) signal accumulations, a series of spectral bunches of lines from C_6F_6–NC_7H_{13}, which are approximately equally spaced, are observed as shown in Figure 2c. This spectral signature matches that of a symmetric top. Each bunch of spectral lines contains different K components, where the quantum number K is the projection of angular momentum on the symmetry axis. Each transition is further split by the nuclear quadrupole hyperfine structure of the nitrogen atom and the internal rotation of the two moieties relative to each other in each cluster. Due to the lower resolution of the broadband spectrum than that of the narrowband spectrum, most of the transitions are blended and indistinguishable in the former.

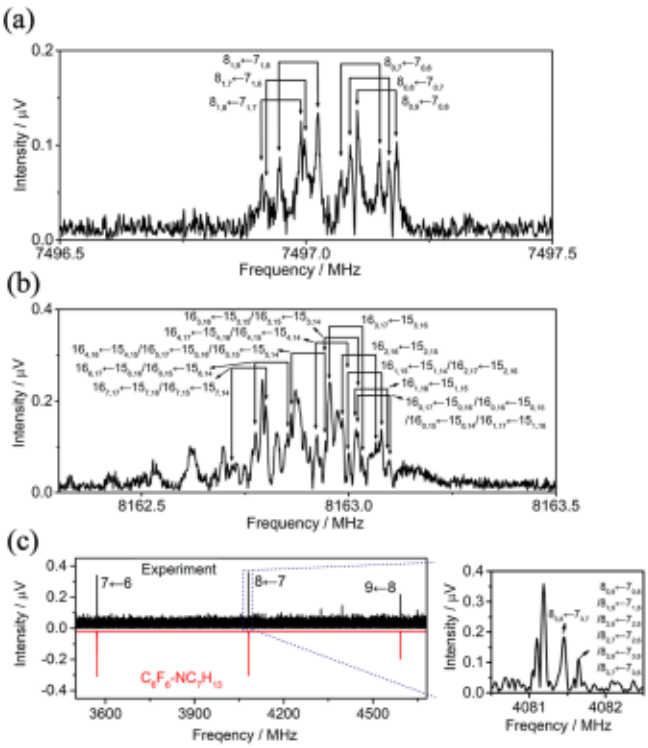

Figure 2. (a) J = 8 ← 7 transitions of C_6F_6–$N(CH_3)_3$, (b) J = 16 ← 15 transitions of C_6F_6–NC_7H_{13} measured by COBRA-FTMW spectrometer. The hyperfine components of transitions $J'_{K',F'} \leftarrow J''_{K'',F''}$ are labeled by the quantum number $F = I + J$. Each component appears as a doublet due to the Doppler effect. (c) $J + 1 \leftarrow J$ (J ranging from 6 to 8) transitions of C_6F_6–NC_7H_{13} measured by CP-FTMW spectrometer. The complete broadband spectra of C_6F_6–$N(CH_3)_3$ and C_6F_6–NC_7H_{13} are available in Figure S2.

In agreement with the theoretical predictions, the rotational spectra of these complexes are assigned to the C_{3v} symmetric rotors. For C_6F_6–$N(CH_3)_3$, several progressions $J + 1 \leftarrow J$ with total angular momentum quantum number J ranging from 8 to 12 are identified. The rotational spectrum of C_6F_6–NC_7H_{13} is obtained for J ranging from 6 to 21. The coupling scheme used for the labeling of the rotational transitions is $F = I + J$, with the nuclear spin quantum number I = 1, associated with the coupling of the nuclear quadrupole moment with the overall molecular rotation. A total of 26 transitions have been assigned

for C_6F_6–$N(CH_3)_3$ within the 6–18 GHz range, while 123 transitions are assigned for C_6F_6–NC_7H_{13} within 2–18 GHz. The measured rotational transitions were fitted using the SPFIT program[50] within the *I*′ representation of Watson's *S* reduction Hamiltonian.[51] Besides the splitting of the spectral lines produced by the ^{14}N nuclear spin and the Doppler effect, some additional weaker lines are observed. The frequencies of these lines are slightly red-shifted from the assigned lines, suggesting that they are associated with lower effective rotational constants. In the complex C_6F_6–NH_3, these lines have been assigned to excited torsional states that arise from the free internal rotation of NH_3 with respect to C_6F_6.[31] For the heavier complexes of C_6F_6–NC_7H_{13} and C_6F_6–$N(CH_3)_3$ in this study, the remaining lines from excited states are too weak and crowed to be identified (as shown in Figure 2a,b). The calculated and experimental spectroscopic constants are listed in Table 1 while all the fitted frequencies are given in

Table 1. Experimental and Calculated Spectroscopic Parameters of C_6F_6–NH_3, C_6F_6–$N(CH_3)_3$, and C_6F_6–NC_7H_{13}, Respectively

	C_6F_6–NH_3[a]	C_6F_6–$N(CH_3)_3$	C_6F_6–NC_7H_{13}
B/MHz	759.6291(1)[b]/ 768.7[c]	468.5774(2)/ 471.3	255.10311(9)/ 255.7
D_J/kHz	0.0910(7)	0.053(9)	0.0147(1)
D_{JK}/kHz	1.899(7)	10.2 (1)	0.2387(7)
H_{KJ}/Hz	−4.3(2)		0.322(4)
D_{Jm}/kHz	67.01(5)		
D_{JKm}/kHz	11.178(1)		
χ_{zz}/MHz	−3.17(2)/−4.14	−5.43(41)/−5.91	−5.15(2)/−5.55
N[d]	157	26	123
σ[e]/kHz	3.2	1.4	6.8

[a]From ref 31. [b]Error in parentheses in units of the last digit. [c]The theoretically calculated (B3LYP-D4/def2-TZVP) rotational and nuclear coupling constants. [d]Number of lines for fit. [e]Standard deviation of the fit.

Tables S4 and S5. The corresponding values for C_6F_6–NH_3 are also given for comparison.[31] The experimental transition frequencies are in good agreement with their calculated values.

Using the theoretical optimized geometry as the initial structure of these complexes, the experimental rotational constants can be reproduced by adjusting the intermolecular distance. This adjusted result is the so-called effective structure of the ground vibrational state (r_0).[52] The comparison of the theoretical and effective values is reported in Figure 1, where the errors in parentheses are given in units of the last digit. The results show that the distance between the N atom and the center of mass (CM) of C_6F_6, r ($N\cdots C_{6F6CM}$), decreases from 3.2685(3) Å in C_6F_6–NH_3, to 3.110(1) Å in C_6F_6–$N(CH_3)_3$, and to 3.040(2) Å in C_6F_6–NC_7H_{13}.

The stretching force constant (k_s) and the dissociation energies (E_D) of the NCI can be estimated for symmetric-top complexes by approximating the complex as comprising two rigid parts. In this pseudodiatomic approximation, the stretching force constant is inversely related to the centrifugal distortion constant by the equation[22,53,54]

$$k_s = 128\pi^4(\mu r_{CM})^2 B^4/(hD_J) \quad (1)$$

where μ, r_{CM}, and D_J are the reduced mass, the distance between the two centers of mass, and the first-order centrifugal distortion constant, respectively. The E_D is evaluated, as shown in Table 2, by assuming a Lennard-Jones potential function, according to equation 2.[55]

$$E_D = 1/72 k_s r_{CM}^2 \quad (2)$$

Table 2. Distances between the Two Centers of Mass (r_{CM}) of the Monomers from the r_0 Structures, Stretching Force Constants (k_s), and Dissociation Energies (E_D) for C_6F_6–NH_3, C_6F_6–$N(CH_3)_3$, and C_6F_6–NC_7H_{13}

	C_6F_6–NH_3	C_6F_6–$N(CH_3)_3$	C_6F_6–NC_7H_{13}
r_{CM}/Å	3.325	3.439	4.320
k_s/N m^{-1}	5.1	11.4	13.5
E_D (Exp)/kJ mol^{-1}	4.7	11.2	21.1
E_D (B3LYP-D4/def2-TZVP)/kJ mol^{-1}	12.9	20.8	22.5

The E_D can also be predicted through quantum chemical calculations. The zero-point energy (ZPE)-corrected[56] values calculated at the B3LYP-D4/def2-TZVP level are also listed in Table 2 for comparison. Even though these values differ from the experimental ones, the increasing trend is in reasonable agreement with the experimental result. Both the experimental and theoretical results show that the binding energy increases with the size of the alkyl substituents. This finding is in agreement with the measured N···π-center distances, which decreases with increasing size of the alkyl substituents.

Based on the analysis of the nuclear quadrupole coupling constants, the spectroscopic evidence of the formation of a lp-π interaction in these complexes can be provided using the valence p-orbital population anisotropy.[57,58] This analysis relies on the extended Townes-Dailey (ETD) model directly relating to the quadrupole coupling tensor.[59] Within the ETD model, only the valence electron population in the p-orbitals contributes to the nuclear quadrupole coupling tensor. If the nuclear quadrupole coupling principal axes and the axes of the p-orbitals coincide, the populations (P) and the nuclear quadrupole coupling constants (χ) are related by equations which contain the population of the orbital and the one-electron contribution to the coupling tensor, χ_0.[60] However, in the case of symmetric tops the relations reduce to a unique equation

$$\chi_{zz} = \chi_0(P_{zz} - P_{xx}) \quad (3)$$

since $P_{xx} = P_{yy}$, and $\chi_{xx} = \chi_{yy} = -\chi_{zz}/2$. In particular, the experimentally derived χ_0 value for ^{14}N is −11.2 MHz,[61] and the orientation of the *x*, *y*, and *z* axes for the present systems is shown in Figure 1.

In the modified ETD model,[57] the *P*-population anisotropies ΔP_{zz} (calculated as differences in orbital population along the *z* axes with respect to the average P_{ave} population) is suggested to quantify the electronic properties

$$\Delta P_{zz} = P_{zz} - P_{ave} \quad (4)$$

where

$$P_{ave} = \frac{1}{3}(P_{xx} + P_{yy} + P_{zz}) \quad (5)$$

Since, for a symmetric top $P_{xx} = P_{yy}$, eq 3 can now be written as

Table 3. Valence p-Orbital Population Anisotropy of the Complexes of C_6F_6–NH_3, C_6F_6–$N(CH_3)_3$, and C_6F_6–NC_7H_{13}

	Experimental		B3LYP-D4/def2-TZVP		
	χ(MHz)	ΔP_{zz}	χ(MHz)	ΔP_{zz}^{χ}	ΔP_{zz}^{NBO}
C_6F_6–NH_3	−3.17(2)	0.189(1)	−4.1408	0.245	0.319
C_6F_6–$N(CH_3)_3$	−5.43(41)	0.323(1)	−5.9087	0.352	0.367
C_6F_6–NC_7H_{13}	−5.15(2)	0.308(1)	−5.5509	0.330	0.378
NH_3	−4.08983(2)[65]	0.243442(1)	−4.2417	0.252	0.332
$N(CH_3)_3$	−5.500(2)[66]	0.327(1)	−5.9385	0.353	0.370
NC_7H_{13}	−5.192(4)[67]	0.309(2)	−5.5722	0.332	0.378

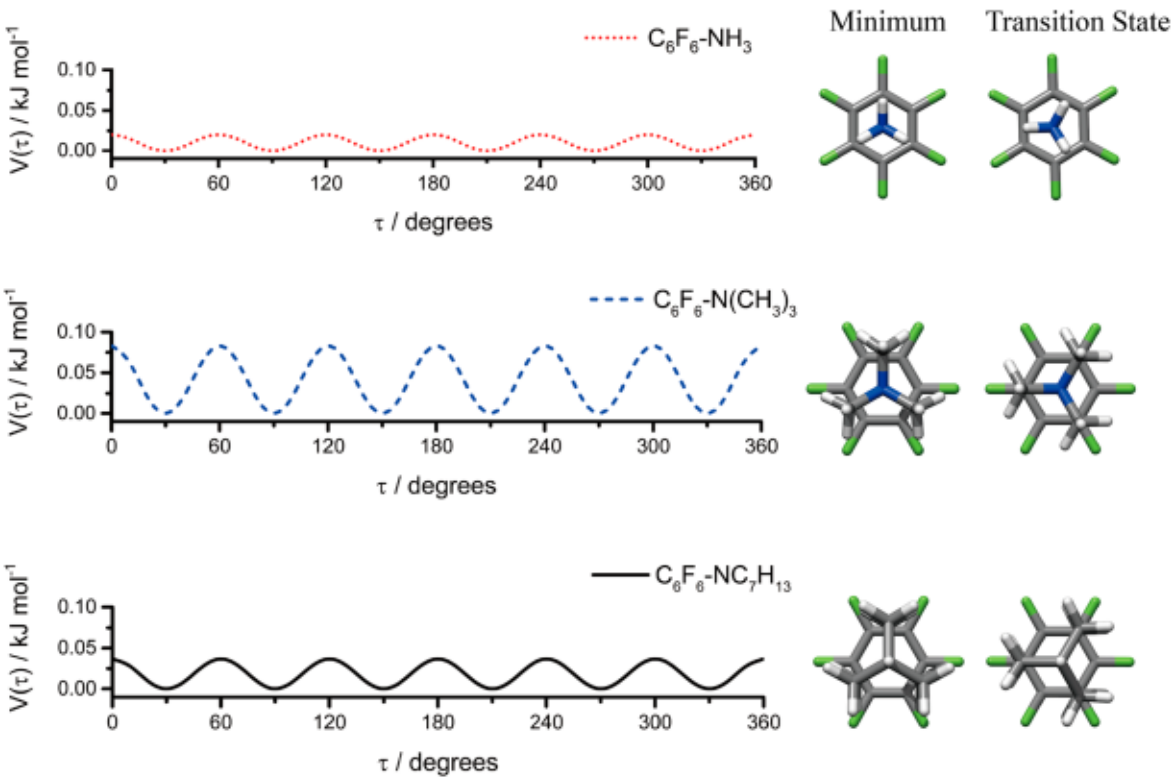

Figure 3. Potential energy functions for the internal rotation of NH_3, $N(CH_3)_3$, and NC_7H_{13} relative to C_6F_6 around their C_3 axes.

$$\chi_{zz} = \frac{3}{2}\chi_0 \Delta P_{zz} \quad (6)$$

Therefore, the *P*-population anisotropy along the nitrogen lone pair direction can be directly estimated from the experimental nuclear quadrupole coupling constant. The χ and ΔP_{zz} values in the three complexes are compared to those of the monomers in Table 3, where also the theoretical values are listed. As regards the *P*-population anisotropy, two series of data are derived: one from the calculated χ (ΔP_{zz}^{χ}) and the other from the NBO[62] analysis of the p-orbitals population (ΔP_{zz}^{NBO}). As already discussed,[57,63] the positive value of ΔP_{zz} is a direct measure of the strong electron density along the *z*-axis, while a negative value indicates a deficiency of electron density (σ-hole) which could lead to interaction with a nucleophilic group. The value of ΔP_{zz} decreases going from the monomer to the complex for C_6F_6–NH_3. This could indicate an electron transfer from the N lone pair to the π-hole, which provides evidence for the formation of lp-π interactions, but it could also be the effect of large-amplitude motions acting on the weakly bound ammonia molecule as shown in ref 64. It is not possible to disentangle these effects, but a close examination of the theoretical values and comparison to the experimental ones can shed some light. Looking at Table 3 we can see that, for all monomers, the quadrupole coupling constants are reasonably reproduced. The differences between the calculated and experimental values are maintained for the complexes of trimethylamine and quinuclidine, while it is larger for the ammonia complex. The larger difference between theoretical and experimental values can be reasonably attributed to the large-amplitude motion's effects sizable for the ammonia complex but not for the other two due to the lower mass of ammonia. Nevertheless, we can also see that, for the ammonia complex, the theoretical values (free of the large-amplitude motion effects) indicate a larger change of the quadrupole coupling constants and ΔP_{zz} in going from monomer to complex. Thus, the change in ΔP_{zz} for the ammonia complex attributed in part to the large-amplitude motion effects and in part to the electronic transfer due to complexation. However, for the other two complexes, the values of ΔP_{zz} remain nearly constant. This can be explained by the electron-donating ability of the alkyl substituents (vide infra), providing a buffer effect.

The potential energy as a function of the orientation of the ligands is calculated theoretically at the B3LYP-D4/def2-TZVP level. The potential energy function for the internal rotation of

NH_3, $N(CH_3)_3$, and NC_7H_{13} relative to C_6F_6 around their C_3 axes is shown in Figure 3. The low barriers being predicted (less than 0.1 kJ mol^{-1}) and the observed symmetric top spectrum is consistent with both $N(CH_3)_3$ and NC_7H_{13} rotating freely with respect to C_6F_6, as previously observed for C_6F_6–H_2O[28] and C_6F_6–NH_3.[31] The internal rotation barriers for $N(CH_3)_3$ and NC_7H_{13} are slightly higher than that of NH_3 with respect to C_6F_6. This result implies the formation of the intermolecular interaction of CH···F in these two larger complexes. These weak CH···F interactions need to be broken and reestablished during the torsion, thereby contributing to the barriers.

To obtain a better visualization of the intermolecular NCIs, Johnson's NCI method is applied.[5] The plots mapping the location and strength of NCIs are shown in Figure 4. The

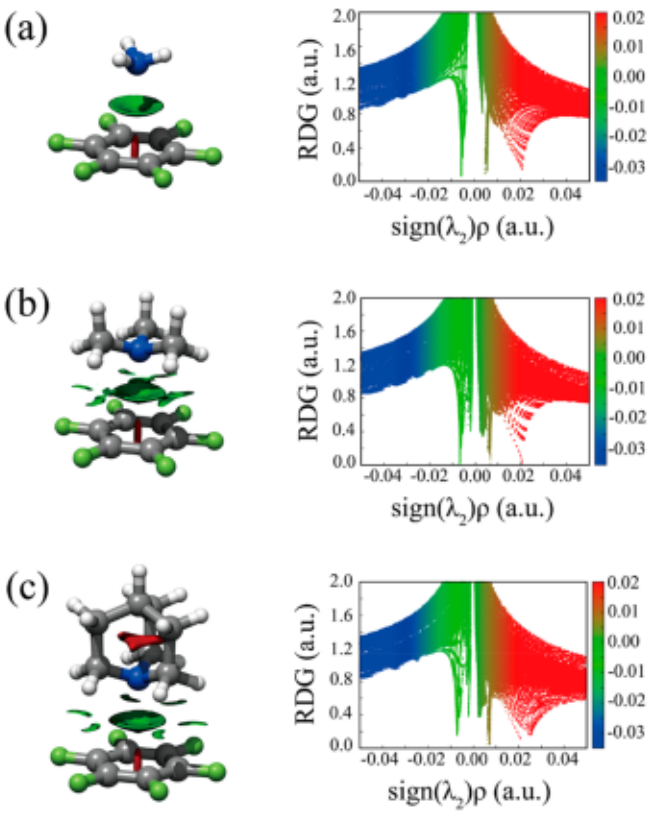

Figure 4. NCI plots from the electron densities (ρ) for (a) C_6F_6–NH_3, (b) C_6F_6–$N(CH_3)_3$, and (c) C_6F_6–NC_7H_{13}, calculated at the B3LYP-D4/def2-TZVP level of theory. Left panel of NCI: reduced density gradient (RDG) isosurfaces colored according to the sign(λ_2)ρ (−0.04–0.04 au). Color coding is blue-green (attractive interactions) and orange-red (repulsive interaction). Right panel of NCI: the RDG versus sign(λ_2)ρ. Positive sign(λ_2)ρ indicates repulsive interaction, and negative sign(λ_2)ρ indicates attractive interaction.

central green circle regions reveal the weak lp-π interactions, whereas the side green regions around the central region in C_6F_6–$N(CH_3)_3$ and C_6F_6–NC_7H_{13} represent the weak CH···F hydrogen bonds which are not present in C_6F_6–NH_3. The CH···F hydrogen bonds become weaker in view of the area size of the NCI plots from C_6F_6–$N(CH_3)_3$ to C_6F_6–NC_7H_{13}. This is consistent with the internal rotation potential function shown in Figure 3. The barrier of C_6F_6–$N(CH_3)_3$ is higher than that of C_6F_6–NC_7H_{13}, which implies that the CH···F hydrogen bonds are stronger in the former complex. This indicates that the stronger overall intermolecular interaction in C_6F_6–NC_7H_{13} compared to C_6F_6–$N(CH_3)_3$ could be attributed to the stronger lp-π interaction in the larger complex.

A quantitative understanding of the chemical nature of the NCIs has been achieved by energy decomposition analysis, using the symmetry-adapted perturbation theory (SAPT).[68] According to SAPT, the energy of the intermolecular interaction can be interpreted as the sum of different terms with defined physical meaning: electrostatic, induction, dispersion, and exchange-repulsion terms. The results summarized in Table S6 and Figure 5 show that the

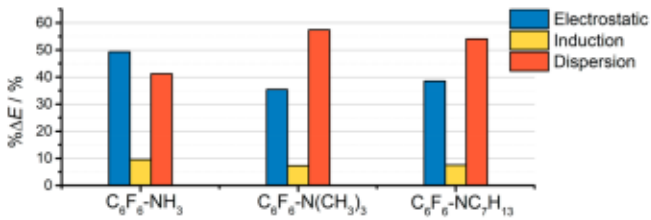

Figure 5. SAPT energy decomposition for the complexes of NH_3, $N(CH_3)_3$, and NC_7H_{13} with C_6F_6. The bar charts show electrostatic, induction, and dispersion energies as a percentage of total attractive interactions of each complex. See Table S6 for detailed values.

intermolecular interactions become stronger with increasing size of the alkyl substituent size. The relative energy scale allows for a general discussion of the driving forces of the different interactions. The electrostatic contribution, suggesting the lp-π interactions, is dominant in the intermolecular interactions of the C_6F_6–NH_3 complex, whereas the London dispersion interactions dominate over the electrostatic interaction in the C_6F_6-alkylamines. This result indicates that the dispersion interactions are mainly responsible for the shorter r (N···C_{6F6CM}) distances when going from C_6F_6–NH_3 to C_6F_6-alkylamines. According to the NCI analysis, the increased dispersions are visualized as a few emerging weak dispersion-dominated CH···F hydrogen bonds.[40,69,70] The dispersion interactions are also related to electron correlations in the whole molecules, and they become stronger as the size of the molecules and the number of electrons increase.[71,72] The higher proportion of electrostatic contribution and lower proportion of dispersion contribution in the intermolecular interactions of C_6F_6–NC_7H_{13} compared to that of C_6F_6–$N(CH_3)_3$ indicates that the lp-π interaction is stronger in C_6F_6–NC_7H_{13} than that in C_6F_6–$N(CH_3)_3$, which coincides with the above analysis. This phenomenon invokes the role of the alkyl group as "electron buffer" that donates electrons to nitrogen as compensation for its consumption in the formation of lp-π interaction. The result is supported by a previous study where the alkylamines with larger alkyl groups tend to be better electron donors due to the electron-donating effect of alkyl groups.[35] In addition, it is consistent with the basicity of NC_7H_{13} (11.14 kcal mol^{-1})[34] being higher than that of $N(CH_3)_3$ (8.82 kcal mol^{-1})[33] in aqueous solution. The electron-donating buffer effect of alkyl substituent also explains why the values ΔP_{zz} of C_6F_6-alkylamines remain constant, instead of decreasing, when complexing with C_6F_6 (Table 3). It is worth noting that the NCI and SAPT results should generally be taken with care, especially in studies where no consistency check with electron distribution sensitive observ-

ables like nuclear quadrupole coupling constant is available, as they might be less reliable as assumed.

In summary, the pure rotational spectra of the C_6F_6–$N(CH_3)_3$ and C_6F_6–NC_7H_{13} complexes have been measured in the 2–18 GHz range. The rotational constants, the centrifugal distortion constants, and nuclear quadrupole coupling constants for both complexes are reported and compared to those of C_6F_6–NH_3. These three complexes exhibit C_{3v} symmetry and undergo internal rotation along their C_3 axes. As the size of the alkyl substituents increases, the N···π-center distance decreases and the intermolecular interaction increases. This phenomenon is attributed to the interplay between dispersion interaction and electrostatic interaction as revealed by the quantitative energy decomposition analysis. The increased intermolecular interaction in going from C_6F_6–NH_3 to C_6F_6-alkylamines is due to the increased dispersion contribution, while the increased intermolecular interaction from C_6F_6–$N(CH_3)_3$ to C_6F_6–NC_7H_{13} is attributed to electrostatic interaction. The values of the P-population anisotropy along the nitrogen lone pair direction (ΔP_{zz}) remain constant during complexing with C_6F_6 for both C_6F_6–$N(CH_3)_3$ and C_6F_6–NC_7H_{13}, while ΔP_{zz} decreases going from NH_3 to the complexes of C_6F_6–NH_3. This result indicates that the alkyl groups act as an "electron buffer" when alkylamines complex with C_6F_6, and the alkyl groups can donate electrons to nitrogen as compensation for its consumption in the formation of lp-π interaction.

■ ASSOCIATED CONTENT

Supporting Information

The Supporting Information is available free of charge at https://pubs.acs.org/doi/10.1021/acs.jpclett.3c00882.

Experimental and theoretical details; The diagram of the CP-FTMW spectrometer at Fudan University; The structural informations of the complexes of C_6F_6–NH_3, C_6F_6–$N(CH_3)_3$, and C_6F_6–NC_7H_{13}; Measured rotational transition frequencies; SAPT analysis (PDF)

■ AUTHOR INFORMATION

Corresponding Authors

Weixing Li − *Department of Chemistry, Collaborative Innovation Center of Chemistry for Energy Materials, Shanghai Key Laboratory of Molecular Catalysis and Innovative Materials, Fudan University, 200438 Shanghai, China;* orcid.org/0000-0003-0169-0990; Email: weixingli@fudan.edu.cn

Luca Evangelisti − *Dipartimento di Chimica "G. Ciamician" - Campus of Ravenna, Università di Bologna, I-48123 Ravenna, Italy;* orcid.org/0000-0001-9119-1057; Email: luca.evangelisti6@unibo.it

Sonia Melandri − *Dipartimento di Chimica "G. Ciamician", Università di Bologna, I-40126 Bologna, Italy;* orcid.org/0000-0002-0410-5833; Email: sonia.melandri@unibo.it

Mingfei Zhou − *Department of Chemistry, Collaborative Innovation Center of Chemistry for Energy Materials, Shanghai Key Laboratory of Molecular Catalysis and Innovative Materials, Fudan University, 200438 Shanghai, China;* orcid.org/0000-0002-1915-6203; Email: mfzhou@fudan.edu.cn

Authors

Dingding Lv − *Department of Chemistry, Collaborative Innovation Center of Chemistry for Energy Materials, Shanghai Key Laboratory of Molecular Catalysis and Innovative Materials, Fudan University, 200438 Shanghai, China;* orcid.org/0000-0002-3998-9667

Imanol Usabiaga − *Dpto. Química Física, Universidad del País Vasco (UPV/EHU), 48940 Leioa, Spain;* orcid.org/0000-0002-1621-8536

Camilla Calabrese − *Dpto. Química Física y Química Inorgánica, Facultad de Ciencias − I.U CINQUIMA, Universidad de Valladolid, 47011 Valladolid, Spain;* orcid.org/0000-0003-4299-2098

Assimo Maris − *Dipartimento di Chimica "G. Ciamician", Università di Bologna, I-40126 Bologna, Italy;* orcid.org/0000-0003-2644-0023

Guanjun Wang − *Department of Chemistry, Collaborative Innovation Center of Chemistry for Energy Materials, Shanghai Key Laboratory of Molecular Catalysis and Innovative Materials, Fudan University, 200438 Shanghai, China;* orcid.org/0000-0002-3265-7192

Complete contact information is available at: https://pubs.acs.org/10.1021/acs.jpclett.3c00882

Author Contributions

The manuscript was written through contributions of all authors. All authors have given approval to the final version of the manuscript.

Notes

The authors declare no competing financial interest.

■ ACKNOWLEDGMENTS

This project is supported by National Natural Science Foundation of China (Grant No. 22103015). W. Li thanks Jens-Uwe Grabow, Luca Evangelisti, and the FS-SMP group for helpful discussions during the construction of the CP-FTMW spectrometer at Fudan University. We thank University of Bologna (RFO) and CINECA award under the ISCRA initiative.

■ REFERENCES

(1) Schneider, H. J. Binding Mechanisms in Supramolecular Complexes. *Angew. Chem., Int. Ed.* **2009**, *48*, 3924–3977.

(2) Persch, E.; Dumele, O.; Diederich, F. Molecular Recognition in Chemical and Biological Systems. *Angew. Chem., Int. Ed.* **2015**, *54*, 3290–3327.

(3) Hobza, P.; Řezáč, J. Introduction: Noncovalent Interactions. *Chem. Rev.* **2016**, *116*, 4911–4912.

(4) de Vries, M. S.; Hobza, P. Gas-Phase Spectroscopy of Biomolecular Building Blocks. *Annu. Rev. Phys. Chem.* **2007**, *58*, 585–612.

(5) Johnson, E. R.; Keinan, S.; Mori-Sánchez, P.; Contreras-Garcia, J.; Cohen, A. J.; Yang, W. Revealing Noncovalent Interactions. *J. Am. Chem. Soc.* **2010**, *132*, 6498–6506.

(6) Li, W.; Spada, L.; Tasinato, N.; Rampino, S.; Evangelisti, L.; Gualandi, A.; Cozzi, P. G.; Melandri, S.; Barone, V.; Puzzarini, C. Theory Meets Experiment for Noncovalent Complexes: The Puzzling Case of Pnicogen Interactions. *Angew. Chem., Int. Ed.* **2018**, *57*, 13853–13857.

(7) Suzuki, S.; Green, P. G.; Bumgarner, R. E.; Dasgupta, S.; Goddard, W. A.; Blake, G. A. Benzene Forms Hydrogen Bonds with Water. *Science* **1992**, *257*, 942–945.

(8) Wang, J.; Spada, L.; Chen, J.; Gao, S.; Alessandrini, S.; Feng, G.; Puzzarini, C.; Gou, Q.; Grabow, J.-U.; Barone, V. The Unexplored

World of Cycloalkene-Water Complexes: Primary and Assisting Interactions Unraveled by Experimental and Computational Spectroscopy. *Angew. Chem., Int. Ed.* **2019**, *58*, 13935−13941.
(9) Li, X.; Spada, L.; Alessandrini, S.; Zheng, Y.; Lengsfeld, K. G.; Grabow, J.-U.; Feng, G.; Puzzarini, C.; Barone, V. Stacked but Not Stuck: Unveiling the Role of $\pi \rightarrow \pi^*$ Interactions with the Help of the Benzofuran−Formaldehyde Complex. *Angew. Chem., Int. Ed.* **2022**, *61*, No. e202113737.
(10) Blanco, S.; López, J. C. Rotational Characterization of an $N \rightarrow \pi^*$ Interaction in a Pyridine−Formaldehyde Adduct. *J. Phys. Chem. Lett.* **2018**, *9*, 4632−4637.
(11) Li, W.; Pérez, C.; Steber, A. L.; Schnell, M.; Lv, D.; Wang, G.; Zeng, X.; Zhou, M. Evolution of Solute−Water Interactions in the Benzaldehyde-$(H_2O)_{1-6}$ Clusters by Rotational Spectroscopy. *J. Am. Chem. Soc.* **2023**, *145*, 4119−4128.
(12) Müller-Dethlefs, K.; Hobza, P. Noncovalent Interactions: A Challenge for Experiment and Theory. *Chem. Rev.* **2000**, *100*, 143−167.
(13) Saleh, G.; Gatti, C.; Lo Presti, L.; Contreras-Garcia, J. Revealing Non-Covalent Interactions in Molecular Crystals through Their Experimental Electron Densities. *Eur. J. Chem.* **2012**, *18*, 15523−15536.
(14) Puzzarini, C.; Spada, L.; Alessandrini, S.; Barone, V. The Challenge of Non-Covalent Interactions: Theory Meets Experiment for Reconciling Accuracy and Interpretation. *J. Phys.: Condens. Matter* **2020**, *32*, 343002−343002.
(15) Obenchain, D. A.; Spada, L.; Alessandrini, S.; Rampino, S.; Herbers, S.; Tasinato, N.; Mendolicchio, M.; Kraus, P.; Gauss, J.; Puzzarini, C.; et al. Unveiling the Sulfur−Sulfur Bridge: Accurate Structural and Energetic Characterization of a Homochalcogen Intermolecular Bond. *Angew. Chem., Int. Ed.* **2018**, *57*, 15822−15826.
(16) Townes, C. H.; Schawlow, A. L. *Microwave Spectroscopy;* Dover: New York, 1975; p 698.
(17) Gordy, W.; Cook, R. L. *Microwave Molecular Spectra;* Wiley: New York, 1984; p 1.
(18) Caminati, W.; Grabow, J.-U. *Advancements in Microwave Spectroscopy;* Elsevier Science, 2018; p 569.
(19) Pate, B. H.; Evangelisti, L.; Caminati, W.; Xu, Y.; Thomas, J.; Patterson, D.; Perez, C.; Schnell, M. *Quantitative Chiral Analysis by Molecular Rotational Spectroscopy;* Elsevier: Amsterdam, The Netherlands, 2018; p 679.
(20) Li, W.; Melandri, S.; Evangelisti, L.; Calabrese, C.; Vigorito, A.; Maris, A. Characterizing Hydrogen and Tetrel Bonds in Clusters of CO_2 with Carboxylic Acids. *Phys. Chem. Chem. Phys.* **2021**, *23*, 16915−16922.
(21) Caminati, W.; Evangelisti, L.; Feng, G.; Giuliano, B. M.; Gou, Q.; Melandri, S.; Grabow, J.-U. On the Cl···C Halogen Bond: A Rotational Study of CF_3Cl-CO. *Phys. Chem. Chem. Phys.* **2016**, *18*, 17851−17855.
(22) López, J. C.; Caminati, W.; Alonso, J. L. The C−H···π Hydrogen Bond in the Benzene−Trifluoromethane Adduct: A Rotational Study. *Angew. Chem., Int. Ed.* **2006**, *45*, 290−293.
(23) Wang, J.; Spada, L.; Chen, J.; Gao, S.; Alessandrini, S.; Feng, G.; Puzzarini, C.; Gou, Q.; Grabow, J.-U.; Barone, V. The Unexplored World of Cycloalkene−Water Complexes: Primary and Assisting Interactions Unraveled by Experimental and Computational Spectroscopy. *Angew. Chem., Int. Ed.* **2019**, *131*, 14073−14079.
(24) Saragi, R. T.; Calabrese, C.; Juanes, M.; Pinacho, R.; Rubio, J. E.; Pérez, C.; Lesarri, A. π-Stacking Isomerism in Polycyclic Aromatic Hydrocarbons: The 2-Naphthalenethiol Dimer. *J. Phys. Chem. Lett.* **2023**, *14*, 207−213.
(25) Egli, M.; Gessner, R. V. Stereoelectronic Effects of Deoxyribose O4′ on DNA Conformation. *Proc. Natl. Acad. Sci. U. S. A.* **1995**, *92*, 180−184.
(26) Gou, Q.; Feng, G.; Evangelisti, L.; Caminati, W. Lone-Pair···π Interaction: A Rotational Study of the Chlorotrifluoroethylene-Water Adduct. *Angew. Chem., Int. Ed.* **2013**, *52*, 11888−11891.
(27) Calabrese, C.; Gou, Q.; Maris, A.; Caminati, W.; Melandri, S. Probing the Lone Pair···π-Hole Interaction in Perfluorinated Heteroaromatic Rings: The Rotational Spectrum of Pentafluoropyridine-Water. *J. Phys. Chem. Lett.* **2016**, *7*, 1513−1517.
(28) Evangelisti, L.; Brendel, K.; Mäder, H.; Caminati, W.; Melandri, S. Rotational Spectroscopy Probes Water Flipping by Full Fluorination of Benzene. *Angew. Chem., Int. Ed.* **2017**, *129*, 13887−13891.
(29) Gou, Q.; Spada, L.; Geboes, Y.; Herrebout, W. A.; Melandri, S.; Caminati, W. N Lone-Pair···π Interaction: A Rotational Study of Chlorotrifluoroethylene···Ammonia. *Phys. Chem. Chem. Phys.* **2015**, *17*, 7694−7698.
(30) López, J. C.; Macario, A.; Maris, A.; Alkorta, I.; Blanco, S. How Aromatic Fluorination Exchanges the Interaction Role of Pyridine with Carbonyl Compounds: The Formaldehyde Adduct. *Eur. J. Chem.* **2021**, *27*, 13870−13878.
(31) Li, W.; Usabiaga, I.; Calabrese, C.; Evangelisti, L.; Maris, A.; Favero, L. B.; Melandri, S. Characterizing the Lone Pair···π-Hole Interaction in Complexes of Ammonia with Perfluorinated Arenes. *Phys. Chem. Chem. Phys.* **2021**, *23*, 9121−9129.
(32) Umeyama, H.; Morokuma, K. Origin of Alkyl Substituent Effect in the Proton Affinity of Amines, Alcohols, and Ethers. *J. Am. Chem. Soc.* **1976**, *98*, 4400−4404.
(33) Jones, F. M., III; Arnett, E. M. Thermodynamics of Ionization and Solution of Aliphatic Amines in Water. In *Progress in Physical Organic Chemistry;* John Wiley & Sons: New York, 1974; pp 263−322.
(34) Aue, D. H.; Webb, H. M.; Bowers, M. T. A Thermodynamic Analysis of Solvation Effects on the Basicities of Alkylamines. An Electrostatic Analysis of Substituent Effects. *J. Am. Chem. Soc.* **1976**, *98*, 318−329.
(35) Huheey, J. E.; Blair, L. K.; Hinze, J.; Whitehead, M. A.; Jaffé, H. Structure and Mechanism in Organic Chemistry. *J. Am. Chem. Soc.* **1971**, *86*, 148−148.
(36) Galera, S.; Oliva, A.; Lluch, J. M.; Bertrán, J. Ab Initio Study of the Solvent Effect on the Basicity of Methylamines. *THEOCHEM* **1984**, *110*, 15−21.
(37) Wagner, J. P.; Schreiner, P. R. London Dispersion in Molecular Chemistry-Reconsidering Steric Effects. *Angew. Chem., Int. Ed.* **2015**, *54*, 12274−12296.
(38) Grimme, S. Dispersion Interaction and Chemical Bonding. In *The Chemical Bond - Chemical Bonding Across the Periodic Table;* John Wiley and Sons: Weinheim, Germany, 2014; p 477.
(39) Quesada-Moreno, M. M.; Schnell, M.; Obenchain, D. A. Rotational Analysis of Naphthol-Aromatic Ring Complexes Stabilized by Electrostatic and Dispersion Interactions. *Phys. Chem. Chem. Phys.* **2022**, *24*, 1598−1609.
(40) Quesada-Moreno, M. M.; Pinacho, P.; Pérez, C.; Šekutor, M.; Schreiner, P. R.; Schnell, M. Do Docking Sites Persist Upon Fluorination? The Diadamantyl Ether-Aromatics Challenge for Rotational Spectroscopy and Theory. *Eur. J. Chem.* **2021**, *27*, 6198−6203.
(41) Ehrlich, S.; Moellmann, J.; Grimme, S. Dispersion-Corrected Density Functional Theory for Aromatic Interactions in Complex Systems. *Acc. Chem. Res.* **2013**, *46*, 916−926.
(42) Neel, A. J.; Hilton, M. J.; Sigman, M. S.; Toste, F. D. Exploiting Non-Covalent π Interactions for Catalyst Design. *Nature* **2017**, *543*, 637−646.
(43) Riley, K. E.; Hobza, P. On the Importance and Origin of Aromatic Interactions in Chemistry and Biodisciplines. *Acc. Chem. Res.* **2013**, *46*, 927−936.
(44) Grimme, S.; Antony, J.; Ehrlich, S.; Krieg, H. A Consistent and Accurate Ab Initio Parametrization of Density Functional Dispersion Correction (DFT-D) for the 94 Elements H-Pu. *J. Chem. Phys.* **2010**, *132*, 154104−154104.
(45) Balle, T. J.; Flygare, W. H. Fabry−Perot Cavity Pulsed Fourier Transform Microwave Spectrometer with a Pulsed Nozzle Particle Source. *Rev. Sci. Instrum.* **1981**, *52*, 33−45.
(46) Grabow, J.-U.; Stahl, W.; Dreizler, H. A Multioctave Coaxially Oriented Beam-Resonator Arrangement Fourier-Transform Microwave Spectrometer. *Rev. Sci. Instrum.* **1996**, *67*, 4072−4084.

(47) Caminati, W.; Millemaggi, A.; Alonso, J. L.; Lesarri, A.; López, J. C.; Mata, S. Molecular Beam Fourier Transform Microwave Spectrum of the Dimethylether−Xenon Complex: Tunnelling Splitting and 131xe Quadrupole Coupling Constants. *Chem. Phys. Lett.* **2004**, *392*, 1−6.
(48) Brown, G. G.; Dian, B. C.; Douglass, K. O.; Geyer, S. M.; Shipman, S. T.; Pate, B. H. A Broadband Fourier Transform Microwave Spectrometer Based on Chirped Pulse Excitation. *Rev. Sci. Instrum.* **2008**, *79*, 53103−53103.
(49) Schmitz, D.; Alvin Shubert, V.; Betz, T.; Schnell, M. Multi-Resonance Effects within a Single Chirp in Broadband Rotational Spectroscopy: The Rapid Adiabatic Passage Regime for Benzonitrile. *J. Mol. Spectrosc.* **2012**, *280*, 77−84.
(50) Pickett, H. M. The Fitting and Prediction of Vibration-Rotation Spectra with Spin Interactions. *J. Mol. Spectrosc.* **1991**, *148*, 371−377.
(51) Watson, J. K. G. In *Vibrational Spectra and Structure;* Durig, J. R., Ed.; Elsevier: New York, 1977; Vol. *6*, pp 1−89.
(52) Kisiel, Z. Least-Squares Mass-Dependence Molecular Structures for Selected Weakly Bound Intermolecular Clusters. *J. Mol. Spectrosc.* **2003**, *218*, 58−67.
(53) Millen, D. J. Determination of Stretching Force Constants of Weakly Bound Dimers from Centrifugal Distortion Constants. *Can. J. Chem.* **1985**, *63*, 1477−1479.
(54) Read, W. G.; Campbell, E. J.; Henderson, G. The Rotational Spectrum and Molecular Structure of the Benzene−Hydrogen Chloride Complex. *J. Chem. Phys.* **1983**, *78*, 3501−3508.
(55) Novick, S. E.; Harris, S. J.; Janda, K. C.; Klemperer, W. Structure and Bonding of Krclf: Intermolecular Force Fields in Van Der Waals Molecules. *Can. J. Phys.* **1975**, *53*, 2007−2015.
(56) Boys, S. F.; Bernardi, F. The Calculation of Small Molecular Interactions by the Differences of Separate Total Energies. Some Procedures with Reduced Errors. *Mol. Phys.* **1970**, *19*, 553−566.
(57) Rinald, A.; Wu, G. A Modified Townes-Dailey Model for Interpretation and Visualization of Nuclear Quadrupole Coupling Tensors in Molecules. *J. Phys. Chem. A* **2020**, *124*, 1176−1186.
(58) Blanco, S.; Pinacho, P.; López, J. C. Structure and Dynamics in Formamide−$(H_2O)_3$: A Water Pentamer Analogue. *J. Phys. Chem. Lett.* **2017**, *8*, 6060−6066.
(59) Cooper, G. A.; Medcraft, C.; Littlefair, J. D.; Penfold, T. J.; Walker, N. R. Halogen Bonding Properties of 4-Iodopyrazole and 4-Bromopyrazole Explored by Rotational Spectroscopy and Ab Initio Calculations. *J. Chem. Phys.* **2017**, *147*, 214303−214303.
(60) Novick, S. E. Extended Townes−Dailey Analysis of the Nuclear Quadrupole Coupling Tensor. *J. Mol. Spectrosc.* **2011**, *267*, 13−18.
(61) Lucken, E. A. C.; Schempp, E. Nuclear Quadrupole Coupling Constants. *Phys. Today* **1970**, *23*, 56−57.
(62) Glendening, E. D.; Reed, A. E.; Carpenter, J. E.; Weinhold, F. *NBO Version 3.1;* Gaussian Inc.: Pittsburgh, PA, 2003.
(63) Lv, D.; Maris, A.; Evangelisti, L.; Maggio, A.; Song, W.; Elliott, A. A.; Peebles, S. A.; Neill, J. L.; Muckle, M. T.; Pate, B. H.; et al. Σ−Hole Activation and Structural Changes Upon Perfluorination of Aryl Halides: Direct Evidence from Gas Phase Rotational Spectroscopy. *Phys. Chem. Chem. Phys.* **2021**, *23*, 18093−18101.
(64) Thomas, J.; Peña, I.; Carlson, C. D.; Yang, Y.; Jäger, W.; Xu, Y. Structural and Dynamical Features of the 2,2,2-Trifluoroethanol··· Ammonia Complex. *Phys. Chem. Chem. Phys.* **2020**, *22*, 23019−23027.
(65) Marshall, M. D.; Muenter, J. S. Stark-Hyperfine Measurements in K = 0 and K = 1 States of NH_3. *J. Mol. Spectrosc.* **1981**, *85*, 322−326.
(66) Li, X. L.; Bocquet, R.; Petitprez, D.; Boucher, D.; Poteau, L.; Demaison, J. The Rotational Spectrum of Trimethylamine Measured by Microwave and Millimeter-Wave Fourier-Transform Spectroscopies and by Sideband Laser Spectroscopy. *J. Mol. Spectrosc.* **1995**, *172*, 449−455.
(67) Consalvo, D.; Stahl, W. The Molecular Structure of Quinuclidine Obtained by High Resolution Microwave Spectroscopy. *J. Mol. Struct.* **1998**, *447*, 119−126.
(68) Jeziorski, B.; Moszynski, R.; Szalewicz, K. Perturbation Theory Approach to Intermolecular Potential Energy Surfaces of Van Der Waals Complexes. *Chem. Rev.* **1994**, *94*, 1887−1930.
(69) Liu, C.-C.; Chan, M. C. W. Chelating Σ-Aryl Post-Metallocenes: Probing Intramolecular [C−H···F−C] Interactions and Unusual Reaction Pathways. *Acc. Chem. Res.* **2015**, *48*, 1580−1590.
(70) Dunitz, J. D.; Gavezzotti, A. Molecular Recognition in Organic Crystals: Directed Intermolecular Bonds or Nonlocalized Bonding? *Angew. Chem., Int. Ed.* **2005**, *44*, 1766−1787.
(71) London, F. Zur Theorie Und Systematik Der Molekularkräfte. *Z. Phys.* **1930**, *63*, 245−279.
(72) London, F. The General Theory of Molecular Forces. *Trans. Faraday Society* **1937**, *33*, 8b−26.